A range-based navigation system for autonomous underwater vehicles

Margarida Pedro

Instituto Superior Técnico - Institute for Systems and Robotics (IST-ISR)
Lisbon, Portugal

October 2014

***Abstract*—Single-beacon range-based navigation systems for underwater vehicles rely on a vehicle's motion to obtain range measurements at different locations in order to estimate its position. This motivates the study of optimal trajectories for improving the accuracy of the position estimate while respecting mission related criteria. The performance index used to compare different trajectories is the determinant of a properly defined Fisher Information Matrix (FIM). Assuming that heading measurements are available, the problem is studied for 2D and 3D, including the case when depth measurements can be obtained. Analytical and numerical solutions are derived. Examples of optimal or close-to-optimal trajectories obtained are (i) circumferences around the beacon for 2D, (ii) cylindrical helices for 3D and (iii) a circumference around the beacon, in the same horizontal plane, for 3D including depth measurements. Additionally for 2D, the case of two vehicles using the same beacon and exchanging range information is studied, for which concentric trajectories that circumnavigate the beacon are shown to be optimal. An approach to deal with the case where the initial position of the vehicle is known to lie in a region of uncertainty is presented. A navigation algorithm consisting of an optimal trajectory planner and a minimum-energy estimator is proposed and tested in the simulation of a practical scientific scenario.**

***Index Terms*—Underwater Range-Based Navigation; Single-Beacon Navigation; Trajectory Optimization; Fisher Information Matrix**

I. Introduction

A. Motivation

In the field of marine robotics, a core problem that arises is the determination of the position and orientation of a vehicle with respect to some inertial reference frame. Several navigation systems exist, based on different working principles and with different advantages and shortcomings. One possible way to find better solutions for underwater navigation is to combine the systems and technologies already available to overcome the individual drawbacks and enhance the advantages of a global system.

Dead reckoning (DR) based and inertial navigation systems estimate the relative change in the vehicle position with errors that are unbounded over time and distance, thus they require auxiliary navigation methods to provide error correction and an absolute georeference [1]. Currently, a common solution is to combine DR or inertial navigation systems with acoustic navigation systems such as LBLs (Long Baseline) or SBLs (Short Baseline), that can provide a position 'fix'. However, these acoustic navigation systems (i) have high operational costs associated with the deployment, calibration or recovery of the acoustic beacons, (ii) lack flexibility because every time the mission location changes the entire system has to be redeployed and recalibrated and (iii) have a limited area of coverage. To overcome some of these shortcomings, in recent years, several publications refer an alternative navigation systems using a single acoustic beacon that provides range measurements to a vehicle [1]–[9]. Briefly, this navigation system consists of a single acoustic source, at a known location, and a moving vehicle that, measuring its ranges to the source, can estimate its position with respect to the source. This solution is a reduced-cost alternative with respect to conventional acoustic systems, like SBL and LBL, that combines the use of a single acoustic beacon with dead reckoning information. The costs are reduced not only because the number of beacons is reduced, but also because the calibration procedure is reduced to the determination of the absolute position of the beacon. On the other hand, single-beacon navigation introduces some difficulties due to the fact that a single range measurement is not enough to define the vehicle position with respect to the beacon. Thus, the vehicle has to move around and acquire range measurements at different positions, while measuring the displacements within measurements, in order to trilaterate its own position. This implies that the navigation system is dependent on the vehicle motion. Thus, this work focuses on studying optimal trajectories for single beacon navigation.

B. Previous Work

One of the first references on single-beacon navigation is [10] where the authors describe the implementation of a navigation system using range data from one acoustic transponder (from a LBL commercial solution) and yaw and relative velocity measurements from on-board sensors. In [2] a similar solution is presented, that relies on very accurate dead reckoning information and uses the range data from a single transponder only as a periodic position 'fix'. In [6], the authors propose an algorithm for 2D homing and navigation that relies on range data from a single source and a 'low-cost' solution for dead reckoning. The algorithm consist of two steps: an initialization phase based on nonlinear least squares and a refinement phase based on an Extended Kalman Filter. They showed convergence and robustness of the navigation system in simulation and post-processing experiments.

The work of [1], [9], [11] approaches the problem of a moving beacon and multiple AUVs that are capable of measuring their ranges to the beacon and use this information for self-localization. In [9] the authors propose a path planing algorithm for the moving beacon that should minimize the position errors accumulated in the other vehicles.

The observability of the single-beacon navigation system using range measurements is studied by [4], [5], [12]–[14],

where different approaches are used to study the observability of the system in a deterministic framework.

Regarding trajectory optimization to improve the accuracy of the navigation system, [15] employs a metric based on the Fisher Information Matrix (FIM) to optimize formation flights with position provided by a range-based navigation system. In [16], the authors describe a metric based on the observability matrix for nonlinear systems, that is used to assess the performance of the 3D single-beacon range-only navigation system, for a static beacon and one vehicle undergoing different trajectories. Finally, [17], [18] use the determinant of the FIM to find the optimal sensor placement that maximizes the accuracy of the localization of a static target using range-only measurements to a set of beacons (sensors).

C. Outline

In section II optimal trajectories for single-beacon range-only navigation are studied in 2D. In section III the problem is approached in 3D. In section IV we introduce the problem of the uncertainty associated with the vehicle initial position. Additionally, an algorithm for a single-beacon range-based navigation is presented. In section V the main conclusions are drawn and possible directions of future work are presented.

II. 2D SINGLE-BEACON NAVIGATION

A. System model

Consider a vehicle moving while measuring its distance $d(t)$ with respect to a stationary beacon. The motion of the vehicle is controlled through its forward speed $v(t) > 0$ and yaw rate $r(t)$. The beacon location is known with respect to some inertial reference frame $\{\mathcal{I}\}$, with North-East-Down orientation (NED). The vehicle has access to the heading angle $\psi(t)$, which provides the orientation of the body frame with respect to the inertial frame $\{\mathcal{I}\}$.

Let the vehicle and the beacon positions in $\{\mathcal{I}\}$ be denoted by $\mathbf{p}(t) = [\, p^n(t) \;\; p^e(t) \,]^T$ and $\mathbf{b_0} = [\, b_0^n \;\; b_0^e \,]^T$ respectively. Without loss of generality, we will assume the beacon to be located at the origin of the reference frame $\{\mathcal{I}\}$, $\mathbf{b}_0 = \mathbf{0}$. Thus, the distance between the vehicle and the beacon is given by

$$d(t) = \|\mathbf{p}(t)\| \tag{II.1}$$

The kinematic model of the system with state $\mathbf{x}(t) = [\, p^n(t) \;\; p^e(t) \;\; \psi(t) \,]^T$, input $\mathbf{u}(t) = [\, v(t) \;\; r(t) \,]^T$ and output $\mathbf{y}(t) = [\, d(t) \;\; \psi(t) \,]^T$ for $t \in [\, 0, t_f \,]$ is given by

$$\dot{\mathbf{x}}(t) = \begin{bmatrix} v(t)\cos(\psi(t)) \\ v(t)\sin(\psi(t)) \\ r(t) \end{bmatrix} \tag{II.2}$$

$$\mathbf{y}(t) = \begin{bmatrix} \|\mathbf{p}(t)\| \\ \psi(t) \end{bmatrix} \tag{II.3}$$

B. Fisher Information Matrix

Let z_i with $i = 0, ..., m-1$ denote a set of m measurements of $d(t)$ corrupted by additive noise, obtained at different time instants t_i. Moreover, let d_i with $i = 0\,,\; ...\,,\; m-1$ denote the actual distances at the time instants of the measurements. The measurement model is given by

$$z_i = d_i + w_i\,, \qquad i = 0\,,\; ...\,,\; m-1 \tag{II.4a}$$

$$w_i \sim \mathcal{N}(0, \sigma^2)\,, \qquad i = 0\,,\; ...\,,\; m-1 \tag{II.4b}$$

Assume that the model introduced in section II-A and the measurement model above describe the system perfectly. Additionally, assume that the initial position of the vehicle $\mathbf{p}_0$ is unknown, but that from the set of measurements $\mathbf{z}$ we can obtain an unbiased estimate $\hat{\mathbf{p}}_0$. Under these assumptions, the determinant of the Fisher Information Matrix (FIM) varies inversely with the volume of the uncertainty ellipsoid of the estimation error. Furthermore, note that if the FIM is nonsingular, the system is observable [19], meaning that trajectories that result from the maximization of the FIM determinant (with $|FIM| > 0$) render the system observable. In the following steps, we derive expressions for the FIM determinant, used later as a performance index for the trajectory optimization.

1) Log-likelihood function: Let $\mathbf{z} = [\, z_0 \;\; z_1 \;\; ... \;\; z_{m-1} \,]^T$ be a vector containing the range measurements, $\mathbf{d} = [\, d_0 \;\; d_1 \;\; ... \;\; d_{m-1} \,]^T$ the corresponding actual ranges and $\mathbf{w} = [\, w_0 \;\; w_1 \;\; ... \;\; w_{m-1} \,]^T$ the corresponding measurement noise samples with $\mathbf{w} \sim \mathcal{N}(\mathbf{0}, R)$ and $R = \sigma^2 I$. Note that the distance $d(t)$ is a function of the position of the vehicle $\mathbf{p}(t)$, that is a function of the vehicle initial position $\mathbf{p}_0$.With some abuse of notation, we denote the vector $\mathbf{d}$ as $\mathbf{d}(\mathbf{p}_0)$ to make the dependence of $\mathbf{p}_0$ explicit.

The likelihood function for the measurement vector with respect to the unknown initial position is given by Equation II.5, from which we derive the log-likelihood function given by Equation II.6.

$$\mathcal{L}_{\mathbf{p}_0}(\mathbf{z}) = \frac{1}{(2\pi)^{\frac{m}{2}}|R|} e^{-\frac{1}{2}(\mathbf{z}-\mathbf{d}(\mathbf{p}_0))^T R^{-1}(\mathbf{z}-\mathbf{d}(\mathbf{p}_0))} \tag{II.5}$$

$$\begin{aligned} \ln \mathcal{L}_{\mathbf{p}_0}(\mathbf{z}) = &-\frac{m}{2}\ln(2\pi) - \ln(|R|) \\ &- \frac{1}{2}\left(\mathbf{z} - \mathbf{d}(\mathbf{p}_0)\right)^T R^{-1}\left(\mathbf{z} - \mathbf{d}(\mathbf{p}_0)\right) \end{aligned} \tag{II.6}$$

Let $J_{\mathbf{p}_0}$ denote the Jacobian matrix taken w.r.t. $\mathbf{p}_0$. The Jacobian of the log-likelihood function w.r.t $\mathbf{p}_0$ is given by

$$J_{\mathbf{p}_0} \ln \mathcal{L}_{\mathbf{p}_0}(\mathbf{z}) = (J_{\mathbf{p}_0}\mathbf{d})^T R^{-1}\left(\mathbf{z} - \mathbf{d}\right) \tag{II.7}$$

2) FIM determinant: The FIM for the problem at hand is defined as

$$FIM_{\mathbf{p}_0} \triangleq E\left\{ \left(J_{\mathbf{p}_0} \ln \mathcal{L}_{\mathbf{p}_0}(\mathbf{z}) \right) \left(J_{\mathbf{p}_0} \ln \mathcal{L}_{\mathbf{p}_0}(\mathbf{z}) \right)^T \right\} \tag{II.8}$$

where $E\{x\}$ denotes the expectation of x. Making use of the previous results, it is given by

$$FIM_{\mathbf{p}_0} = \frac{1}{\sigma^2}(J_{\mathbf{p}_0}\mathbf{d})^T(J_{\mathbf{p}_0}\mathbf{d}) \tag{II.9}$$

with

$$(J_{\mathbf{p}_0}\mathbf{d}) = \begin{bmatrix} \frac{p_0^n}{d_0} & \dots & \frac{p_{m-1}^n}{d_{m-1}} \\ \frac{p_0^e}{d_0} & \dots & \frac{p_{m-1}^e}{d_{m-1}} \end{bmatrix}^T \tag{II.10}$$

where $\mathbf{p}_i = [\, p_i^n \quad p_i^e \,]^T$ and d_i denote the position of the vehicle and range to the beacon at $t = t_i$, respectively.

The FIM can be rewritten as

$$FIM_{\mathbf{p}_0} = \frac{1}{\sigma^2}\begin{bmatrix} \sum_{i=0}^{m-1}\left(\frac{p_i^n}{d_i}\right)^2 & \sum_{i=0}^{m-1}\left(\frac{p_i^n}{d_i}\right)\left(\frac{p_i^e}{d_i}\right) \\ \sum_{i=0}^{m-1}\left(\frac{p_i^n}{d_i}\right)\left(\frac{p_i^e}{d_i}\right) & \sum_{i=0}^{m-1}\left(\frac{p_i^e}{d_i}\right)^2 \end{bmatrix} \tag{II.11}$$

hence, the determinant of the FIM is given by

$$|FIM_{\mathbf{p}_0}| = \frac{1}{\sigma^4}\left[\sum_{i=0}^{m-1}\left(\frac{p_i^n}{d_i}\right)^2\sum_{i=0}^{m-1}\left(\frac{p_i^e}{d_i}\right)^2 - \left(\sum_{i=0}^{m-1}\frac{p_i^n}{d_i}\frac{p_i^e}{d_i}\right)^2\right] \tag{II.12}$$

C. Trajectory optimization

In this section we study the trajectories that maximize the FIM determinant which, by construction, maximize the accuracy of the initial vehicle position estimate.

1) Problem Setup:

Assumption 1.: The vehicle speed is constant and the yaw rate is piecewise constant,

$$v(t) = \bar{v} \tag{II.13}$$

$$r(t) = r_k, \text{ for } t_k \le t < t_{k+1}, \ k = 0, ..., N-1 \tag{II.14}$$

with $|r_k| \le r_b$, where r_b is a bound on the vehicle yaw rate that should be set in accordance with the characteristics of specific vehicles.

Assumption 2.: The time instants at which the inputs may change are given by $t_k = k\,T$, for $k = 0, ..., N-1$, with T the cycle interval.

In view of the above, the vehicle position at any t can be written as a function of $\mathbf{p}_0$, ψ_0, $\bar{v}$, $\mathbf{r} = (\, r_0 \,,\, r_1 \,,\, \dots \,,\, r_{N-1}\,)$ and T, given by

$$\mathbf{p}(t) = \mathbf{p}_0 + \bar{v}\sum_{j=0}^{k-1}\frac{1}{r_j}\begin{bmatrix}\sin(\psi((j+1)\,T)) - \sin(\psi(j\,T))\\ -\cos(\psi((j+1)\,T)) + \cos(\psi(j\,T))\end{bmatrix} + \frac{\bar{v}}{r_k}\begin{bmatrix}\sin(\psi(t)) - \sin(\psi(k\,T))\\ -\cos(\psi(t)) + \cos(\psi(k\,T))\end{bmatrix} \tag{II.15a}$$

$$\psi(t) = \psi_0 + T\sum_{j=0}^{k-1} r_j + (t - k\,T)\,r_k \tag{II.15b}$$

$$k = \text{floor}(t/T) \tag{II.15c}$$

where the function $\text{floor}(x)$ returns the largest integer not greater than x. If any r_k is zero the expression for $\mathbf{p}(t)$ has a singularity, which is removable.

Assumption 3.: The time instants at which the range measurements are obtained are given by $t_i = i\,\Delta t$, for $i = 0, ..., m-1$, with Δt the sampling interval.

Assumption 4.: The cycle interval of the yaw rate function, T, is a multiple of Δt. We introduce a new tuning parameter c, such that $T = c\,\Delta t$.

The vehicle positions and the actual ranges, at the time instants t_i, are given by Equations II.15 for $t = i\Delta t$ and $T = c\Delta t$. Hence, the FIM determinant is fully defined as a function of the problem parameters and variables, which are summarized in Table II.1.

setup parameters	$\mathbf{p}_0$, ψ_0, Δt, m, σ, c, $\bar{v}$, r_b
problem variables	$r_0, ..., r_{N-1}$, with $N = \frac{m-1}{c}$

Table II.1: Setup parameters and optimization variables.

Note that the speed $\bar{v}$ is a parameter because small AUVs usually keep the speed approximately constant during missions; a typical value is 1.5 ms^{-1}. The bound on the yaw rate is set to $20\,^\circ s^{-1}$, a typical value from the MEDUSA [1].

[1]MEDUSA is a small AUV for scientific research, from Instituto Superior Técnico/Institute for System and Robotics

2) Maximizing the FIM determinant: The problem of maximizing the FIM determinant including the vehicle dynamics explicitly is too complex for an analytical solution to be obtained for a general scenario. Therefore, first we look for a solution in two steps: (i) find the optimal locations for the measurement points neglecting the vehicle dynamics and (ii) find trajectories that can cover all the optimal measurement points and check if those are compatible with the vehicle dynamics. Later, using numerical procedures, we find trajectories that maximize the FIM determinant including the vehicle dynamics explicitly.

a) Optimal measurement points: Remember the FIM determinant given by Equation II.12. Note that the terms $\frac{p_i^n}{d_i}$ and $\frac{p_i^e}{d_i}$ on the determinant equation represent the cosine and sine, respectively, of the angle between the axis pointing north and the position vector of the vehicle, α_i. Then, consider two new variables $\Gamma_1 \triangleq [\cos(\alpha_0) \ \dots \ \cos(\alpha_{m-1})]^T$ and $\Gamma_2 \triangleq [\sin(\alpha_0) \ \dots \ \sin(\alpha_{m-1})]^T$. Note that

$$\sum_{i=0}^{m-1}\left(\frac{p_i^n}{d_i}\right)^2 = \sum_{i=0}^{m-1}\cos^2(\alpha_i) = \|\Gamma_1\|^2 \tag{II.16}$$

$$\sum_{i=0}^{m-1}\left(\frac{p_i^e}{d_i}\right)^2 = \sum_{i=0}^{m-1}\sin^2(\alpha_i) = \|\Gamma_2\|^2 \tag{II.17}$$

and

$$\sum_{i=0}^{m-1}\left(\frac{p_i^n}{d_i}\right)\left(\frac{p_i^e}{d_i}\right) = \sum_{i=0}^{m-1}\cos(\alpha_i)\sin(\alpha_i) = \|\Gamma_1\|\|\Gamma_2\|\cos(\Theta) \tag{II.18}$$

where Θ is the angle between Γ_1 and Γ_2. Additionally note that

$$\|\Gamma_1\|^2 = m - \|\Gamma_2\|^2 \tag{II.19}$$

Hence, the FIM determinant can be rewritten as

$$|FIM_{\mathbf{p}_0}| = \sigma^{-4}\|\Gamma_1\|^2\left(m - \|\Gamma_1\|^2\right)\sin^2(\Theta) \tag{II.20}$$

and maximizing the FIM determinant is equivalent to

$$\max_{\|\Gamma_1\|,\Theta} \quad \|\Gamma_1\|^2\left(m - \|\Gamma_1\|^2\right)\sin^2(\Theta) \tag{II.21}$$

The first order optimality conditions yield

$$\frac{\partial|FIM_{\mathbf{p}_0}|}{\partial\|\Gamma_1\|} = \|\Gamma_1\|\left(m - 2\|\Gamma_1\|^2\right)\sin^2(\Theta) = 0 \tag{II.22a}$$

$$\frac{\partial|FIM_{\mathbf{p}_0}|}{\partial\Theta} = \|\Gamma_1\|\left(m - \|\Gamma_1\|^2\right)\sin(\Theta)\cos(\Theta) = 0 \tag{II.22b}$$

The solutions for the system of Equations II.22 are given by

$$\left(\cos(\Theta^*) = 0 \wedge \|\Gamma_1^*\|^2 = \frac{m}{2}\right) \vee \sin(\Theta^*) = 0 \vee \|\Gamma_1^*\| = 0$$

By substituting the solutions in Equation II.20, it becomes clear that the FIM determinant is maximum for $\cos(\Theta^*) = 0$ and $\|\Gamma_1^*\|^2 = \frac{m}{2}$; and due to the equality given by Equation II.19 we have $\|\Gamma_2^*\|^2 = \frac{m}{2}$. Thus, the maximum of the determinant of the FIM is given by

$$|FIM_{\mathbf{p}_0}|^* = \left(\frac{m}{2\sigma^2}\right)^2$$

and the corresponding FIM

$$FIM_{\mathbf{p}_0}^* = \left(\frac{m}{2\sigma^2}\right)^2 I_2$$

Note that the two eigenvalues of $FIM^*_{\mathbf{p}_0}$ are equal. Thus, the solution that maximizes the FIM determinant also maximizes the condition number (the ratio between the minimum and maximum eigenvalues). Furthermore, recall that the determinant of a matrix equals the product of its eigenvalues. If another solution existed with greater minimum eigenvalue, the determinant would necessarily be bigger than the optimal, which is not possible. Thus, this solution also maximizes the minimum eigenvalue.

The optimal solution satisfies

$$\sum_{i=0}^{m-1} \cos(\alpha_i)\sin(\alpha_i) = 0 \tag{II.23a}$$

$$\sum_{i=0}^{m-1} \cos^2(\alpha_i) = \frac{m}{2} \tag{II.23b}$$

$$\sum_{i=0}^{m-1} \sin^2(\alpha_i) = \frac{m}{2} \tag{II.23c}$$

Invoking the orthogonality conditions for sines and cosines, from Fourier Analysis, we notice that one family of solutions for the optimal measurement points is given by

$$\sum_{i=0}^{m-1} \cos(\alpha_i)\sin(\alpha_i) = 0 \tag{II.24a}$$

$$\sum_{i=0}^{m-1} \cos^2(\alpha_i) = \sum_{i=0}^{m-1} \cos^2\left(\frac{2\pi p}{m} i\right) \tag{II.24b}$$

$$\sum_{i=0}^{m-1} \sin^2(\alpha_i) = \sum_{i=0}^{m-1} \sin^2\left(\frac{2\pi p}{m} i\right) \tag{II.24c}$$

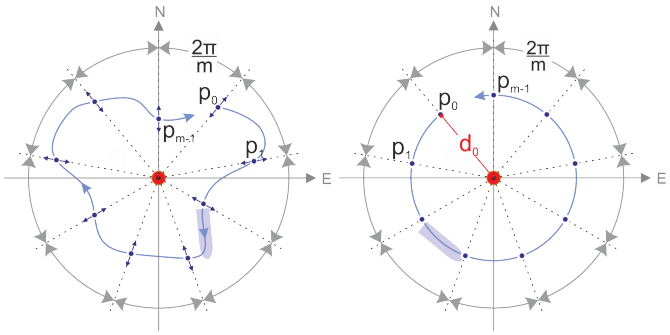

(a) General form. (b) Constant turning rate.

Figure II.1: Optimal trajectories for maximizing the FIM determinant imposing no limitations on the input functions.

Figure II.1a represents the general form of one family solutions for the problem in hands. From Equations II.24, it comes clear that the optimality conditions are fulfilled if the optimal measurement points are radially distributed around the beacon; the optimality of the solution does not depend on the distance of the points to the beacon, neither on their time sequence. Additionally, the solution remains optimal (i) if any of these points is replaced by its reflection with respect to the beacon or (ii) if all points suffer an equal rotation centered in the beacon. Note that combining all the properties of this family of solutions the possible shapes of different trajectories that fulfill the conditions given by Equations II.24 become untraceable. Figure II.1b depicts an optimal solution with constant turning rate and maintaining a fixed distance to the beacon. Finally, note that other solutions may exists that are not in the form of the orthogonality conditions for sines and cosines, but that still fulfill the optimality conditions.

b) Constant speed and piece-wise constant yaw rate: The vehicle kinematics is now included explicitly in the trajectory optimization. Because of the increased complexity of the optimization problem, numerical procedures from the Global Optimization Toolbox of MATLAB are used.

The problem of finding the trajectories that maximize the FIM determinant is equivalent to finding the set of N values for the optimization variables that maximizes the FIM determinant

$$\max_{r_0,\ldots,r_{N-1}} \quad |FIM_{\mathbf{p}_0}| \tag{II.25}$$

subject to

$$|r_k| \leq r_b, \qquad \text{for} \quad k = 0, ..., N-1 \tag{II.26}$$

with $|FIM_{\mathbf{p}_0}|$ given by Equation II.12 and defined as a function of the optimization variables and setup parameters by Equations II.15. Table II.2 shows the results obtained

Scenario	ψ_0 [rad]	r_b [º/s]	$\sigma^4\|FIM\|$
1	$\frac{\pi}{2}$	20	64.00
2	0	20	38.00
3	0	40	59.30

Table II.2: Setup parameters used in the numerical optimization of the FIM determinant and the value of the FIM determinant obtained for each solution.

with the numerical procedure for different scenarios, with $\mathbf{p}_0 = (10, 0)\ [m]$, $\Delta t = 1\ s$, $m = 16$, $c = 1$, $\bar{v} = 1.5\ ms^{-1}$ and the remaining setup parameters defined in the table. First, let us stress that the optimal FIM determinant obtained in section II-C2a, equal to $\frac{m^2}{4\sigma^4}$, sets an upper bound on the performance achievable considering constraints on input function. Analyzing Table II.2 we see that, for scenario 1, the limits imposed by the vehicle dynamics did not preclude the optimization procedure from finding a trajectory with maximum performance. On the other hand, for scenarios 2 and 3, the constraints imposed on the vehicle maneuverability degrades the navigation system performance (in comparison to the optimal situation). Thus, we conclude that the effect of the limitations of the vehicle dynamics on the achievable performance (in terms of the FIM determinant) depends on the setup parameters, this is, the initial conditions, $\mathbf{p}_0$ and ψ_0, and the parameters m, c and Δt.

3) Minimizing energy consumption: In this section, trajectories that simultaneously maximize the FIM determinant and minimize the energy consumption along the trajectory will be derived. Since we intend to obtain general results, applicable to a wide variety of vehicles, the energy criterion we will use is based on very general principles that are in accordance with the kinematic model used in this chapter. Consider that the energy consumption while the vehicle is moving in mainly used to overcome the drag forces F_D and drag torques τ_D. Because v and r are constant or piece-wise constant for the trajectories considered, we have $P_F \propto |v|^3$ and $P_\tau \propto |r|^3$ (P_F and P_τ denote the power of drag forces and torques, respectively). Neglecting the additional energy

spent in changing the yaw rate, the basic model of energy consumption is given by

$$P(t) = \beta\,|\bar{v}|^3 + \gamma\,|r(t)|^3, \qquad \beta,\gamma > 0 \tag{II.27}$$

Because the speed in not an optimization variable, the energy criterion for the optimization is given by $E = \int_0^{t_f} |r(t)|^3 dt$ which, for the piece-wise constant yaw rate function, can be written as

$$E = c\,\Delta t \sum_{j=0}^{N-1} |r_j|^3 - (Nc - m)\;\Delta t\,|r_{N-1}|^3 \tag{II.28}$$

Combining the energy criterion with the FIM determinant criterion in a single optimization problem results on a multicriteria optimization problem. In mathematical terms the problem is formulated as

$$\max_{r_0,\ldots,r_{N-1}} \; (\,|FIM_{\mathbf{p}_0}|\,,\; -E\,) \tag{II.29}$$

subject to Equation II.26. To solve this optimization problem we resorted to the Multicriteria Optimization Toolbox from MATLAB. Figure II.2 shows the results of the optimization

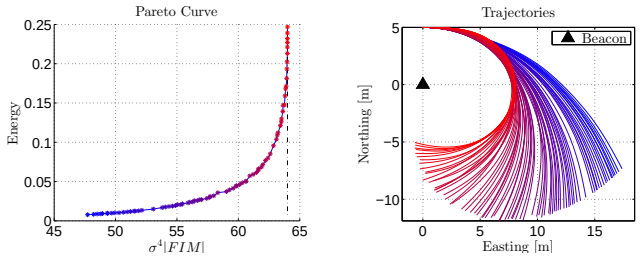

Figure II.2: Pareto curve and the trajectories corresponding to each optimal solution (in the same color) for the problem of minimizing the FIM determinant and the energy consumption by the vehicle.

for $\mathbf{p}_0 = (5,0)\;[m]$, $\psi_0 = \frac{\pi}{2}\;rad$, $\Delta t = 1\;s$, $m = 16$, $c = 1$, $\bar{v} = 1.5\;ms^{-1}$ and $r_b = 20\;^\circ s^{-1}$. The plot on the left shows the Pareto optimal solutions and a Pareto curve obtained by connecting the solutions points (blue line). The plot on the right shows the trajectories associated to each of the Pareto solutions, using the same color. Notice that blue represents trajectories with less energy consumption while red represents trajectories with higher energy consumption by the vehicle. The trade-off between the two objectives of the optimization is very clear (i) minimizing the energy consumption leads directly to the reduction of the absolute values of the yaw rate which decreases the vehicle ability to circumnavigate the beacon, thus reflecting in lower values of the FIM determinant; (ii) nevertheless note that the FIM determinant reaches its maximum value while the energy function continues increasing its value which means that there is a point where increasing the absolute value of the yaw rate does not improve the performance of the navigation system.

4) Minimizing the deviation from a nominal trajectory: In a real situation, we expect the underwater vehicle to perform a useful mission while it tries to estimate its position (using, for example, a range-only positioning system). Motivated by these requirements, we addressed the case where the vehicle should follow a nominal trajectory, but at the same time it is given some freedom so that it can improve the position estimate accuracy. We denote the nominal trajectory by $\mathbf{p}_n(t) : [0, t_f] \rightarrow \mathbb{R}^2$ and the actual trajectory by $\mathbf{p}(t) : [0, t_f] \rightarrow \mathbb{R}^2$, both defined in $\{\mathcal{I}\}$. The deviation from the nominal trajectory is defined as the integral of the squared position error along the trajectory $\delta = \int_0^{t_f} \|\mathbf{p}_n(t) - \mathbf{p}(t)\|^2\,dt$. The optimization problem is formulated as

$$\max_{r_0,\ldots,r_{N-1},\bar{v}} \quad \mu_1\,|FIM_{\mathbf{p}_0}| - \mu_2\,\delta \tag{II.30}$$

subject to Equation II.26 and $0 \leq \bar{v} \leq \bar{v}_{ub}$, with μ_1 and μ_2 weighting factors. To force the final point of the solution trajectory to be close-enough to the final point of the nominal trajectory we added an extra cost to the squared position error concerning the last points of the two trajectories, and included the forward speed as an optimization variable. Figures II.3a and II.3b show two solutions resulting from

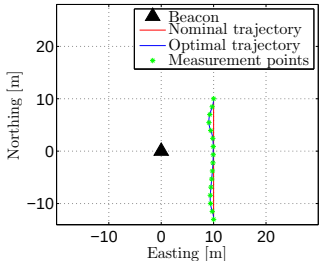

(a) $\mu_1 = 10$ and $\mu_2 = 1$.

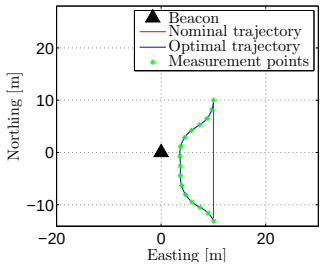

(b) $\mu_1 = 20$ and $\mu_2 = 1$.

Figure II.3: Trajectories that maximize the FIM determinant while minimizing the deviation from a nominal trajectory - linear motion.

the numerical optimization, for different weighting factors between the objective functions, μ_1 and μ_2. The setup parameters are $\mathbf{p}_0 = (10,10)\;[m]$, $\psi_0 = \pi\;rad$, $\Delta t = 1\;s$, $m = 16$, $c = 1$, $r_b = 20\;^\circ s^{-1}$ and $\bar{v}_u b = 2\;ms^{-1}$; and the nominal trajectory is defined by a constant speed $\bar{v}_{nom} = 1.5\;ms^{-1}$, $\mathbf{r}_{nom} = \mathbf{0}$ and $\psi_{nom} = \psi_0$. Obtaining the range measurements along the nominal trajectory, with sampling interval Δt, yields $\sigma^4|FIM|_{nom} = 50.05$, which is already close to the maximum achievable value $\sigma^4|FIM|^* = 64$ (for $m = 16$). Nevertheless, the slight oscillation that we see in Figure II.3a is enough to improve the performance to $\sigma^4|FIM|_{\mu_1=10,\mu_2=1} = 52.44$. Furthermore, the trajectory in Figure II.3b allows for the performance to reach $\sigma^4|FIM|_{\mu_1=20,\mu_2=1} = 63.09$, although it deviates considerably from the nominal trajectory. In practice, the trade-off between the two objective functions depends on the requirements of specific missions.

D. Two vehicles exchanging range information

1) System configuration: Consider the scenario depicted in Figure II.4 of two vehicles using the same beacon for

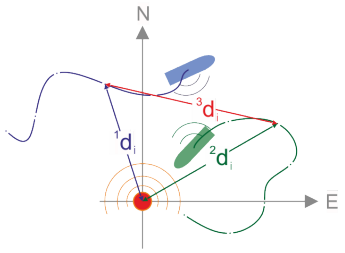

Figure II.4: Single-beacon navigation with two vehicles exchanging range information.

navigation while exchanging range information. The two vehicles have the kinematic model introduced in Equation II.2. Let (i) the vehicle 1 position be denoted by ${}^1\mathbf{p}(t) = [\,{}^1p^n(t) \;\; {}^1p^e(t)\,]^T$; (ii) the vehicle 2 position be denoted by ${}^2\mathbf{p}(t) = [\,{}^2p^n(t) \;\; {}^2p^e(t)\,]^T$; (iii) the beacon fixed position be denoted by $\mathbf{b} = [\,b^n \;\; b^e\,]^T$. Without loss of generality, we hold the assumption of fixing the beacon position at $\mathbf{b} = \mathbf{0}$. Moreover, let the distances between each vehicle and the beacon and between vehicles be denoted as ${}^1d(t) = \|{}^1\mathbf{p}(t)\|$, ${}^2d(t) = \|{}^2\mathbf{p}(t)\|$ and ${}^3d(t) = \|{}^2\mathbf{p}(t) - {}^1\mathbf{p}(t)\|$, respectively. Consider that as the vehicles move, they get measurements of these distances with the following measurement models

$$ {}^1z_i = {}^1d_i + {}^1w_i\,, \qquad {}^1w_i \sim \mathcal{N}(0, {}^1\sigma^2) \tag{II.31a} $$
$$ {}^2z_i = {}^2d_i + {}^2w_i\,, \qquad {}^2w_i \sim \mathcal{N}(0, {}^2\sigma^2) \tag{II.31b} $$
$$ {}^3z_i = {}^3d_i + {}^3w_i\,, \qquad {}^3w_i \sim \mathcal{N}(0, {}^3\sigma^2) \tag{II.31c} $$

for $i = 0, ..., m-1$, where ${}^1z_i$, ${}^2z_i$ and ${}^3z_i$ denote the measurements samples; ${}^1d_i$, ${}^2d_i$ and ${}^3d_i$ denote samples of the actual distances ${}^1d(t)$, ${}^2d(t)$ and ${}^3d(t)$, respectively; ${}^1w_i$, ${}^2w_i$ and ${}^3w_i$ denote the measurement errors samples; and m denotes the number of samples.

2) Trajectory Optimization: Given the problem configuration introduced before, we wish to find what types of trajectories should the two vehicles follow in order to maximize the FIM determinant. To obtain a solution for the optimal locations for the measurement points, we follow the same steps showed for the problem with 1 vehicle. Because of the complexity of the expressions and the computations, those are omitted here. The optimality conditions that the measurement points have to verify in order to maximize the FIM determinant for this problem are given by

$$ \sum_{i=0}^{m-1} \left(\frac{{}^1p_i^n}{{}^1d_i}\right)^2 = \sum_{i=0}^{m-1} \left(\frac{{}^1p_i^e}{{}^1d_i}\right)^2 = \frac{m}{2} \tag{II.32a} $$

$$ \sum_{i=0}^{m-1} \left(\frac{{}^2p_i^n}{{}^2d_i}\right)^2 = \sum_{i=0}^{m-1} \left(\frac{{}^2p_i^e}{{}^2d_i}\right)^2 = \frac{m}{2} \tag{II.32b} $$

$$ \sum_{i=0}^{m-1} \left(\frac{{}^2p_i^n - {}^1p_i^n}{{}^3d_i}\right)^2 = \sum_{i=0}^{m-1} \left(\frac{{}^2p_i^e - {}^1p_i^e}{{}^3d_i}\right)^2 = \frac{m}{2} \tag{II.32c} $$

$$ \sum_{i=0}^{m-1} \left(\frac{{}^1p_i^n}{{}^1d_i}\right)\left(\frac{{}^1p_i^e}{{}^1d_i}\right) = 0 \tag{II.32d} $$

$$ \sum_{i=0}^{m-1} \left(\frac{{}^2p_i^n}{{}^2d_i}\right)\left(\frac{{}^2p_i^e}{{}^2d_i}\right) = 0 \tag{II.32e} $$

$$ \sum_{i=0}^{m-1} \left(\frac{{}^2p_i^n - {}^1p_i^n}{{}^3d_i}\right)\left(\frac{{}^2p_i^e - {}^1p_i^e}{{}^3d_i}\right) = 0 \tag{II.32f} $$

We can easily see that the conditions that concern each of the vehicles alone (Equations II.32a,II.32b, II.32d and II.32e) are the same the conditions obtained for the problem concerning one single vehicle. This indicates that the same type of trajectories that we have seen to be solution of the problem for one single vehicle in Section II-C2a, may also be solution of this problem. We now investigate under what conditions these trajectories fulfill the remaining conditions (Equations II.32c and II.32f). To help us understand the geometric structure of the problem we introduce Figure II.5. Note that

$$ \frac{{}^1p_i^n}{{}^1d_i} = \cos({}^1\alpha_i) \qquad \frac{{}^1p_i^e}{{}^1d_i} = \sin({}^1\alpha_i) $$
$$ \frac{{}^2p_i^n}{{}^2d_i} = \cos({}^2\alpha_i) \qquad \frac{{}^2p_i^e}{{}^2d_i} = \sin({}^2\alpha_i) $$
$$ \frac{{}^2p_i^n - {}^1p_i^n}{{}^3d_i} = \cos({}^1\alpha_i + {}^3\alpha_i) \qquad \frac{{}^2p_i^e - {}^1p_i^e}{{}^3d_i} = \sin({}^1\alpha_i + {}^3\alpha_i) $$

Then it becomes clear that if ${}^3\alpha_i = k\pi, k \in \mathbb{Z}$ for all

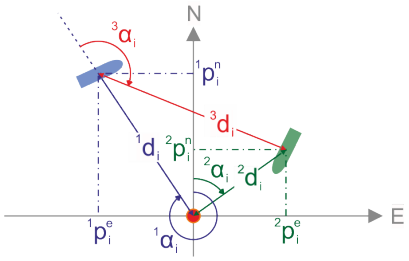

Figure II.5: Geometric insight on the two vehicles problem.

$i \in \{0, ...m-1\}$, the conditions given by the Equations II.32c and II.32f are fulfilled as long as the conditions that concern vehicle 1 are fulfilled (Equations II.32a and II.32d). This corresponds to requiring that the two vehicles obtain the range measurements at the same radials, as depicted in Figure II.6a. The optimality of this solution is invariant to rotations around the beacon and it is not dependent on the distance of the vehicles to the beacon, and neither on the distance between the vehicles. In Figure II.6b we represent the solution that renders the trajectories to be circular. If the vehicles have the same turning rate, the speed and the radius of the two trajectories are related by $({}^1v/{}^1d) = ({}^2v/{}^2d)$.

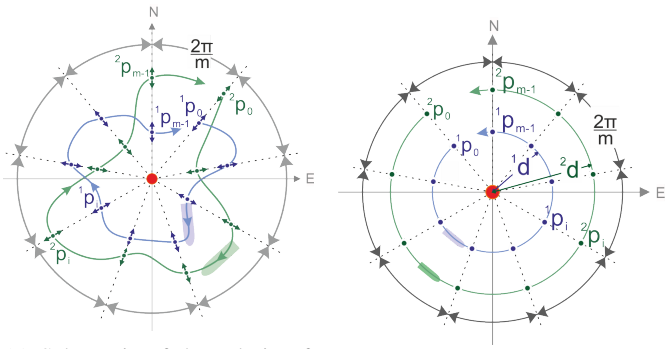

(a) Schematic of the solution for the two vehicles problem.

(b) Circular motion.

Figure II.6: Solution for the 2 vehicles problem.

Moreover, let the variance of the range measurements ${}^1d_i$, ${}^2d_i$ and ${}^3d_i$, for all $i \in \{0, ...m-1\}$, be the same and equal

to σ^2, the variance of the range measurements in the problem of one vehicle. In these conditions, the optimal value of the FIM determinant is $|FIM_{1\mathbf{p}_0,^2\mathbf{p}_0}|^* = \left(\frac{3}{4}\frac{m}{\sigma^2}\right)^2$. Given the optimal FIM determinant for the problem of 1 vehicle alone, $|FIM_{\mathbf{p}_0}|^* = \left(\frac{m}{2\sigma^2}\right)^2$, we can see that $|FIM_{1\mathbf{p}_0,^2\mathbf{p}_0}|^* > 2|FIM_{\mathbf{p}_0}|^*$, which means that the cooperation between the two vehicles improves slightly the degree of observability of the the system.

III. 3D SINGLE-BEACON NAVIGATION BASED ON RANGE MEASUREMENTS

This section extends the problem of single-beacon navigation using range information to 3D. An analogous approach to 2D is followed here, with the required adaptations to 3D. To avoid repeating all the derivations only the differences between 2D and 3D are highlighted.

A. System model

Consider the system introduced in Section II-A. The flight-path-angle $\gamma(t) : [0, t_f] \rightarrow \left[-\frac{\pi}{2}, \frac{\pi}{2}\right]$ is introduced as an input, which is measured with respect to the horizontal plane and is positive when the vehicle is diving. The new kinematic model of the 3D system has state $\mathbf{x}(t) = \left[p^n(t)\ p^e(t)\ p^d(t)\ \psi(t)\right]^T$, input $\mathbf{u}(t) = \left[v(t)\ r(t)\ \gamma(t)\right]^T$ and output $\mathbf{y}(t) = \left[d(t)\ \psi(t)\right]^T$. The system equations for $t \in [0, t_f]$ are given by

$$\dot{\mathbf{x}}(t) = \begin{bmatrix} v(t)\cos(\gamma(t))\cos(\psi(t)) \\ v(t)\cos(\gamma(t))\sin(\psi(t)) \\ v(t)\sin(\gamma(t)) \\ r(t) \end{bmatrix} \tag{III.1}$$

$$\mathbf{y}(t) = \begin{bmatrix} \|\mathbf{p}(t)\| \\ \psi(t) \end{bmatrix} \tag{III.2}$$

with p^d the vertical coordinate of the position. The beacon remains located at the origin of the inertial reference frame $\{\mathcal{I}\}$ (NED oriented), thus $\mathbf{b_0} = \mathbf{0}$. Note that the distance between the vehicle and the beacon is still given by Equation II.1, but now $d(t)$ denotes the 3D Euclidean norm of the position vector.

B. Fisher Information Matrix

Following the same steps as for 2D we derive the FIM and its determinant. The latter is given by

$$\begin{aligned} |FIM(\mathbf{p}_0)| = \\ \sum_{i=0}^{m-1}\left(\frac{p_i^n}{d_i}\right)^2 \left[\sum_{i=0}^{m-1}\left(\frac{p_i^e}{d_i}\right)^2 \sum_{i=0}^{m-1}\left(\frac{p_i^d}{d_i}\right)^2 - \left(\sum_{i=0}^{m-1}\frac{p_i^e}{d_i}\frac{p_i^d}{d_i}\right)^2\right] - \\ \sum_{i=0}^{m-1}\frac{p_i^n}{d_i}\frac{p_i^e}{d_i}\left[\sum_{i=0}^{m-1}\frac{p_i^n}{d_i}\frac{p_i^e}{d_i}\sum_{i=0}^{m-1}\left(\frac{p_i^d}{d_i}\right)^2 - \sum_{i=0}^{m-1}\frac{p_i^n}{d_i}\frac{p_i^d}{d_i}\sum_{i=0}^{m-1}\frac{p_i^e}{d_i}\frac{p_i^d}{d_i}\right] \\ + \sum_{i=0}^{m-1}\frac{p_i^n}{d_i}\frac{p_i^d}{d_i}\left[\sum_{i=0}^{m-1}\frac{p_i^n}{d_i}\frac{p_i^e}{d_i}\sum_{i=0}^{m-1}\frac{p_i^e}{d_i}\frac{p_i^d}{d_i} - \sum_{i=0}^{m-1}\frac{p_i^n}{d_i}\frac{p_i^d}{d_i}\sum_{i=0}^{m-1}\left(\frac{p_i^e}{d_i}\right)^2\right] \end{aligned} \tag{III.3}$$

C. Trajectory optimization

As before, the performance index used to compare different trajectories is the FIM determinant.

1) Optimal measurement points: The optimization problem can be formulated as

$$\max \quad |FIM_{\mathbf{p}_0}| \tag{III.4}$$

with $|FIM_{\mathbf{p}_0}|$ given by Equation III.3. Following the same methodology as for 2D the optimality conditions for the locations of the measurement points are derived. Those are given by

$$\sum_{i=0}^{m-1}\left(\frac{p_i^n}{d_i}\right)^2 = \sum_{i=0}^{m-1}\left(\frac{p_i^e}{d_i}\right)^2 = \sum_{i=0}^{m-1}\left(\frac{p_i^d}{d_i}\right)^2 = \frac{m}{3} \tag{III.5a}$$

$$\sum_{i=0}^{m-1}\frac{p_i^n}{d_i}\frac{p_i^e}{d_i} = \sum_{i=0}^{m-1}\frac{p_i^n}{d_i}\frac{p_i^d}{d_i} = \sum_{i=0}^{m-1}\frac{p_i^e}{d_i}\frac{p_i^d}{d_i} = 0 \tag{III.5b}$$

with optimal FIM determinant given by

$$|FIM^*| = \left(\frac{m}{3\,\sigma^2}\right)^3 \tag{III.6}$$

Similarly to the solution for 2D, one family of solutions that satisfies the optimality conditions renders the measurement points to be radially distributed around the beacon. This family of solutions has the same properties as the optimal solution found for 2D. Regarding the possible shapes of the trajectories that fulfill these optimality conditions, none of the usual candidates, *lines*, *circumferences* and *cylindrical helices*, are adequate. Nevertheless, next we now that cylindrical helices, can achieve very good performances in terms of the FIM determinant, close to optimal.

2) Cylindrical helices - close-to-optimal trajectories: These trajectories are obtained by fixing the control inputs and yield constant values for speed v, yaw rate r and flight-path angle γ. As such, they are convenient for many applications.

For $v(t) = \bar{v}$, $r(t) = \bar{r}$ and $\gamma(t) = \bar{\gamma}$, nonzero constants, the measurements points and corresponding actual ranges are given by

$$\mathbf{p}_i = \mathbf{p}_0 + \bar{v}\begin{bmatrix} \frac{\cos(\bar{\gamma})}{\bar{r}}\left(\sin(\psi_0 + \bar{r}\,i\,\Delta t) - \sin(\psi_0)\right) \\ \frac{\cos(\bar{\gamma})}{\bar{r}}\left(-\cos(\psi_0 + \bar{r}\,i\,\Delta t) + \cos(\psi_0)\right) \\ \sin(\bar{\gamma})\,i\,\Delta t \end{bmatrix} \tag{III.7a}$$

$$d_i = \|\mathbf{p}_i\| \tag{III.7b}$$

for $i = 0, ..., m-1$.

Finding the helix parameters that maximize the FIM determinant corresponds to solving the following optimization problem

$$\max_{\bar{v},\bar{r},\bar{\gamma}} \quad |FIM(\mathbf{p}_0)| \tag{III.8}$$

with $|FIM(\mathbf{p}_0)|$ defined as a function of the setup parameters (Δt, $\mathbf{p}_0$ and ψ_0) and optimization variables ($\bar{v}$, $\bar{r}$ and $\bar{\gamma}$) by Equations III.3 and III.7.

No constraints on the input functions: Table III.1 shows the results of the numerical optimization for different scenarios, with $\Delta t = 1$. The setup parameters that generate each of the trajectories as well as the trajectory parameters $\bar{v}$, $\bar{r}$ and $\bar{\gamma}$ and the ratio between the maximum achievable FIM determinant and the FIM determinant for the trajectory, q_{FIM},

are described. A first look at the table reveals that all the trajectories, even with different setup parameters, achieve very good performance. A more detailed analysis shows that when the number of samples increases, the module of the speed and yaw rate required to achieve close-to-optimal performance decreases. A simple explanation for this fact is that when the number of samples increases, the time that the vehicle has available to circumnavigate the beacon also increases.

	$\mathbf{p}_0$[m]	ψ_0[º]	m	$\bar{v}$[m/s]	$\bar{r}$[º/s]	$\bar{\gamma}$[º]	q_{FIM}
1	$1,1,1$	315	3	2.9	-0.1	-119.8	0.98
2	$1,1,1$	315	10	2.1	4.6	-43.1	0.99
3	$1,1,1$	315	50	0.3	3.5	-7.9	0.99
4	$10,10,10$	0	3	16.9	-12.7	-76.8	0.83
5	$10,10,10$	0	10	6.6	-13.4	-32.5	0.90
6	$10,10,10$	0	50	2.1	-11.4	-10.8	0.99

Table III.1: Setup parameters and results of the optimization of helices to maximize the FIM determinant.

Considering the vehicle dynamics: Consider the optimization problem defined above subject to (i) $0 \leq \bar{v} \leq v_{ub}$, (ii)$|\bar{r}| \leq r_b$ and $|\bar{\gamma}| \leq \frac{\pi}{2}$, with $v_{ub} = 2$ m/s and $r_b = 20$ º/s. Solutions obtained from a numerical optimization procedure, for $\mathbf{p}_0 = (1,1,1)$ m, $\Delta t = 1$ s and $\psi_0 = 315$ º, are presented in Table III.2. Comparing the results in Table III.2

	m	$\bar{v}$ [m/s]	$\bar{r}$ [º/s]	$\bar{\gamma}$ [º]	q_{FIM}
1	10	0.52	1.14	-20	0.28
2	20	0.59	2.42	-19.1	0.99

Table III.2: Setup parameters and results of the optimization of helices to maximize the FIM determinant, imposing limits on the input functions.

with the results in Table III.1 (obtained with no constraints on the input functions), it becomes clear that the inclusion of these constraints may degrade the performance. Additionally, comparing the two results obtained considering the vehicle dynamics (in Table III.2), since the only difference between the two cases is the number of samples m, a natural explanation for the different performance is that the vehicle dynamics may not allow for the vehicle to cover all the optimal measurement points within a limited time interval. Increasing the number of samples, the optimal measurement points remain radially distributed around the beacon, but the vehicles has more time to circumnavigation the beacon. Thus, for a bigger number of samples, even considering the vehicle dynamics, it is possible to find cylindrical helices that exhibit close-to-optimal performance in terms of the FIM determinant, as in case 2 of Table III.2.

D. A realistic assumption: known depth

The availability of depth measurements simplifies the position estimation by discarding the need for the vertical component of the position to be estimated through the range information. Moreover, depth sensors are quite affordable, when compared to other navigation equipment and, therefore, an option in many applications. Thus, we study the optimal trajectories for this scenario. The output of the system given by Equation III.1 becames

$$\mathbf{y}(t) = \begin{bmatrix} \|\mathbf{p}(t)\| \\ \psi(t) \\ p^d(t) \end{bmatrix} \tag{III.9}$$

and the FIM determinant is given by Equation II.12, but with d_i representing the 3D ranges.

1) Trajectory Optimization: The trajectories obtained numerically for maximizing the FIM determinant indicate that the performance improves when the vehicle is in the same horizontal plane as the beacon. When the vehicle dynamics allows it, the vehicle moves into the plane of the beacon and circumnavigates it.

2) Moving on a plane of constant depth: If we consider the 3D problem, with depth measurements, constrained to a plane of constant depth, it resembles the 2D problem considerably. Most important, it covers several practical scenarios that require the AUVs to move at approximately constant depth such as, for instance, in oil and gas surveys.

The analysis of the FIM determinant for this scenario provides the following results: (i) the optimal solution requires the vehicle to move on a circumference in the same horizontal plane where the beacon is located; (ii) for any other horizontal plane, the optimal solution consists on a circumference centered on the vertical projection of the beacon position on that plane and with a radius as large as possible.

IV. Single-beacon navigation under uncertainty in the initial position

In this section the problem of having some uncertainty associated with the initial position estimate is introduced. An algorithm for single-beacon navigation, that deals with that problem and provides optimal trajectories, is developed and tested in simulation for a practical scenario.

A. Uncertainty in the initial position of the vehicle

We approached the problem of obtaining an optimal trajectory for the region of uncertainty by maximizing the worst case scenario. An alternative would have been to maximize the expected value of the FIM determinant along the uncertainty region. However, the chosen approach guarantees a minimum performance. The problem is solved considering that the uncertainty in the vehicle position concerns only the horizontal components, because this scenario assumes that depth measurements are available.

We model the uncertainty region as a circle of center $c_0 = [\ c_0^n\ c_0^e\ ]^T$ and radius r_0. Thus, the problem can be formulated as

$$\max_{\mathbf{r}} \min_{\mathbf{p}_0 \in \mathcal{U}} \quad |FIM(\mathbf{p}_0, \mathbf{r})| \tag{IV.1}$$

subject to Equation II.26, with the $|FIM|$ defined as a function of $\mathbf{r}$ and $\mathbf{p}_0$ by the Equations II.12 and II.15. Due to the complexity of this problem, we (i) resort to numerical methods to obtain a solution and (ii) discretize the uncertainty region $\mathcal{U}$ into a set of points inside and on the boundary of the circle. The performance of the trajectories provided by this procedure depends a lot on location an dimension of the uncertainty region and on the setup parameters. The performance of those trajectories was compared with randomly generated trajectories, and the first consistently outscored the latter significantly.

B. An algorithm for single-beacon navigation

In this section we describe a navigation algorithm for single-beacon navigation using range, depth and heading measurements. The algorithm includes a trajectory planner and a position estimator working on a loop. Its structure is as follows: given a certain initial estimate of the state of the system and corresponding initial covariance matrix, (i) the trajectory planner provides the system speed, yaw rate and flight-path angle commands for an optimal trajectory; (ii) the position estimator observes the outputs of the system (range, depth and heading) and provides an estimate of the vehicle position and the associated uncertainty and (iii) based on that information the trajectory planner recomputes the optimal trajectory, restarting the loop.

C. Minimum-energy state estimator

In what follows we resort to the use of minimum-energy estimator to compute the position of the vehicle. The reader is referred to [20] for the details, which we omit here. The dynamics of the minimum-energy estimator with estimate vector $\hat{\mathbf{x}} = [\ \hat{p}^n\ \ \hat{p}^e\ \ \hat{p}^d\ \ \hat{d}^2\ ]^T$, are given by

- for $t_i \leq t < t_{i+1}$, $i = 0, ..., l$

$$\dot{Q}(t) = -Q(t)\,A(t) - A^T(t)\,Q(t) - Q(t)\,\Gamma\,Q(t) + C_c^T(t)\,R_c^{-1}\,C_c(t) \tag{IV.2}$$

$$\dot{\hat{x}}(t) = \mathbf{f}(\hat{\mathbf{x}}(t), \mathbf{u}(t)) + Q^{-1}(t)\,C_c^T(t)\,R_c^{-1}\Big(\mathbf{y}_c(t) - \mathbf{h}_c(\hat{\mathbf{x}}(t), \mathbf{u}(t))\Big) \tag{IV.3}$$

- at $t = t_{i+1}$, $i = 0, ..., l-1$

$$Q(t_{i+1}) = Q(t_{i+1}^-) + C_d^T(t_{i+1}^-)\,R_d^{-1}\,C_d(t_{i+1}^-) \tag{IV.4}$$

$$\hat{\mathbf{x}}(t_{i+1}) = \hat{\mathbf{x}}(t_{i+1}^-) + Q^{-1}(t_{i+1})\,C_d^T\,(t_{i+1}^-)\,R_d^{-1}\cdot \cdot\Big(\mathbf{y}_d(t_{i+1}) - h_d(\hat{\mathbf{x}}(t_{i+1}^-), \mathbf{u}(t_{i+1}^-))\Big) \tag{IV.5}$$

with

$$\mathbf{f}(\hat{\mathbf{x}}(t), \mathbf{u}(t)) = \begin{bmatrix} v(t)\cos(\gamma(t))\cos(\psi(t)) \\ v(t)\cos(\gamma(t))\sin(\psi(t)) \\ v(t)\sin(\gamma(t)) \\ r(t) \end{bmatrix} \tag{IV.6}$$

$$\mathbf{h}_c(\hat{\mathbf{x}}(t), \mathbf{u}(t)) = \begin{bmatrix} p^d(t) \\ \psi(t) \end{bmatrix} \tag{IV.7}$$

$$h_d(\hat{\mathbf{x}}(t), \mathbf{u}(t)) = (p^n(t))^2 + (p^e(t))^2 + (p^d(t))^2 \tag{IV.8}$$

$$A(t) = \begin{bmatrix} 0 & 0 & 0 & -v(t)\cos(\gamma(t))\sin(\psi(t)) \\ 0 & 0 & 0 & v(t)\cos(\gamma(t))\cos(\psi(t)) \\ 0 & 0 & 0 & 0 \\ 0 & 0 & 0 & 0 \end{bmatrix} \tag{IV.9}$$

$$C_c(t) = \begin{bmatrix} 0 & 0 & 1 & 0 \\ 0 & 0 & 0 & 1 \end{bmatrix} \tag{IV.10}$$

$$C_d(t) = \begin{bmatrix} 2p^n(t) & 2p^e(t) & 2p^d(t) & 0 \end{bmatrix} \tag{IV.11}$$

and $Q(0) = Q_0$ and $\hat{\mathbf{x}}(0) = \hat{\mathbf{x}}_0$ the initial information matrix and state estimate, respectively.

D. Trajectory planner

For the trajectory planner we use a similar approach to [6], in the sense that the algorithm consists of two phases:

1) For a certain, predefined, time interval, the vehicle moves with the single purpose of improving the position estimate. To this effect we employ the maximization procedure introduced in Section IV-A, but with the required modification to include the 3D model.
2) Given a nominal trajectory that the vehicle should follow, the trajectory planner provides a trajectory that does not deviate much from the nominal trajectory, but ensures enough 'excitation' for the estimation procedure. To meet this objective, we employ the optimization procedure introduced in Section II-C4, with the proper modifications to consider the system in 3D, with depth measurements available.

Using the the information matrix and position estimate provided by the observer, the uncertainty region is defined as a circle on the horizontal plane of center $\hat{\mathbf{p}}$ and radius based on the Q matrix. When the radius of the uncertainty region duplicates or reduces to half, a new trajectory is planned.

E. A practical scenario: simulation results

One of the goals in underwater scientific research is to have, in a near future, several underwater labs for monitoring the biodiversity, data collection in general or in-site experiments, to name only a few applications. An example of these labs is the already existing NOOA Aquarius Reef Base [21], in Florida U.S.A. For deep-waters, one practical difficulty is the access to those labs, since using human divers is impractical. Fortunately, the advances in AUV technology allow for AUVs to take care of the interaction between the researchers on the surface and the underwater lab. This is the scenario where we propose to test the navigation algorithm, in simulation. It consists of a underwater lab, 1000 meters below the sea surface equipped with an acoustic beacon. An AUV is launched at the see surface with an initial estimate of the state $\hat{\mathbf{x}}_0$ and covariance Q_0^{-1} (w.r.t the NED frame with origin at the lab). The AUV homes in on the lab and docks there to collect the available data. To this effect, it uses the navigation algorithm developed in this chapter, by measuring its range to the lab. To complete the phase 1 of the algorithm, the vehicle has 5 minutes, in which it should improve the position estimate. For phase 2 the nominal trajectory consists of three straight lines: (i) one vertical part, that covers half of the remaining vertical distance to the lab; (ii) one part with constant flight-path angle and heading angle; and (iii) one horizontal part with the same constant heading as the previous part, that covers half of the horizontal distance to lab when phase 2 begins. Figure IV.1 shows the trajectories resulting from the simulation with Gaussian noise of variance $10\ m^2$ corrupting the range measurements. The filter parameters are $\Gamma = 0$, $R_c = diag([0.01\ 1])$ and $R_d = 0.01$. The estimates for north and east coordinates are initialized $100\ m$ apart from the true coordinates. When the position estimate indicates that the vehicle reached the lab, the true position is $20\ cm$ apart. If more precision is required for docking, short-range auxiliary systems can be used, such as cameras.

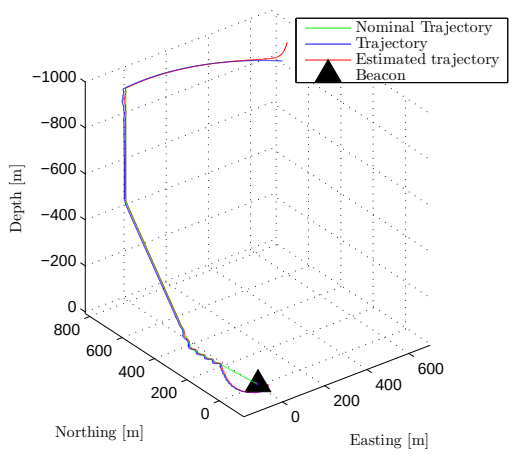

Figure IV.1: Simulation results - trajectories.

V. Conclusions and Future Work

A. Conclusions

This work approached the problem of trajectory optimization for single-beacon navigation using range measurements. To measure the accuracy of the position estimate that a certain trajectory provides, the determinant of FIM was used.

For 2D, the optimal trajectories, in general, render the vehicle to circumnavigate the beacon. That is still valid when considering two vehicles exchanging range information, with the additional condition that the trajectories of the two vehicle should be parallel. Regarding the minimization of the energy consumption, the results show that the general trend is that, reducing the energy consumption by the vehicle decreases the maneuverability, leading to a worst performance in terms of the determinant of the FIM. The procedure designed for planning optimal trajectories that are a trade-off between following as close as possible some nominal trajectory and maximizing the FIM determinant was shown that, for most scenarios, the accuracy of the position estimate can be improved with minimal deviation from the nominal trajectory.

The conclusions for the problem in 3D problem are similar. In general, a trajectory is optimal if the measurement points are radially distributed around the beacon. Additionally, the 3D problem considering depth measurements available was tackled, and the results indicate that the optimal scenario consists of the vehicle moving in the same horizontal plane where the beacon is located.

Finally, a 3D navigation algorithm that combines an optimal trajectory planner with a minimum-energy estimator was presented. A major achievement of the trajectory planner is that it includes the uncertainty associated with the position estimate explicitly. The algorithm was tested in simulation for a practical scenario and the results indicate that it is appropriated for the scenario purpose and similar ones.

B. Future work

On a theoretical perspective, a possible next step is to design an estimator that can ensure that the estimate converges to the true position. It would also be interesting to compare results obtained with different estimators, using optimal trajectories as defined in this thesis. On a practical perspective, an experimental validation of the navigation algorithm would be a natural follow-up to this work, including an experimental analysis of the achievable performance in terms of the accuracy of the position estimate.

References

[1] S. Webster, R. Eustice, H. Singh, and L. Whitcomb, "Preliminary deep water results in single-beacon one-way-travel-time acoustic navigation for underwater vehicles," in *Intelligent Robots and Systems, 2009. IROS 2009. IEEE/RSJ International Conference on*, Oct 2009, pp. 2053–2060.

[2] M. Larsen, "Synthetic long baseline navigation of underwater vehicles," in *OCEANS 2000 MTS/IEEE Conference and Exhibition*, vol. 3, 2000, pp. 2043–2050 vol.3.

[3] R. M. Eustice, H. Singh, and L. L. Whitcomb, "Synchronous-clock, one-way-travel-time acoustic navigation for underwater vehicles," *Journal of Field Robotics*, vol. 28, no. 1, pp. 121–136, 2011. [Online]. Available: http://dx.doi.org/10.1002/rob.20365

[4] A. Gadre and D. Stilwell, "A complete solution to underwater navigation in the presence of unknown currents based on range measurements from a single location," in *Intelligent Robots and Systems, 2005. (IROS 2005). 2005 IEEE/RSJ International Conference on*, Aug 2005, pp. 1420–1425.

[5] P. Batista, C. Silvestre, and P. Oliveira, "Single range aided navigation and source localization: Observability and filter design," *Systems I& Control Letters*, vol. 60, no. 8, pp. 665 – 673, 2011. [Online]. Available: http://www.sciencedirect.com/science/article/pii/S0167691111001174

[6] P. Baccou and B. Jouvencel, "Homing and navigation using one transponder for auv, postprocessing comparisons results with long base-line navigation," in *Robotics and Automation, 2002. Proceedings. ICRA'02. IEEE International Conference on*, vol. 4. IEEE, 2002, pp. 4004–4009.

[7] J. C. Hartsfield, "Single transponder range only navigation geometry (strong) applied to remus autonomous under water vehicles," 2005.

[8] C. E. LaPointe, "Virtual long baseline (vlbl) autonomous underwater vehicle navigation using a single transponder," Ph.D. dissertation, 2006.

[9] M. Chitre, "Path planning for cooperative underwater range-only navigation using a single beacon," in *Autonomous and Intelligent Systems (AIS), 2010 International Conference on*. IEEE, 2010, pp. 1–6.

[10] A. Scherbatyuk, "The auv positioning using ranges from one transponder lbl," in *OCEANS '95. MTS/IEEE. Challenges of Our Changing Global Environment. Conference Proceedings.*, vol. 3, Oct 1995, pp. 1620–1623 vol.3.

[11] M. F. Fallon, G. Papadopoulos, J. J. Leonard, and N. M. Patrikalakis, "Cooperative auv navigation using a single maneuvering surface craft," *The International Journal of Robotics Research*, p. 0278364910380760, 2010.

[12] N. Crasta, M. Bayat, A. P. Aguiar, and A. M. Pascoal, "Observability analysis of 2d single beacon navigation in the presence of constant currents for two classes of maneuvers," in *Control Applications in Marine Systems*, vol. 9, no. 1, 2013, pp. 227–232.

[13] G. Indiveri and G. Parlangeli, "Further results on the observability analysis and observer design for single range localization in 3d," *arXiv preprint arXiv:1308.0517*, 2013.

[14] N. Crasta, M. Bayat, A. P. Aguiar, and A. M. Pascoal, "Observability analysis of 3d auv trimming trajectories in the presence of ocean currents using single beacon navigation," 2014.

[15] P. Huxel and T. U. of Texas at Austin, *Navigation Algorithms and Observability Analysis for Formation Flying Missions*. University of Texas at Austin, 2006. [Online]. Available: http://books.google.pt/books?id=r_fcnBYH0i4C

[16] F. Arrichiello, G. Antonelli, A. P. Aguiar, and A. Pascoal, "Observability metric for the relative localization of auvs based on range and depth measurements: theory and experiments," in *Intelligent Robots and Systems (IROS), 2011 IEEE/RSJ International Conference on*. IEEE, 2011, pp. 3166–3171.

[17] D. Salinas, "Adaptive sensor networks for mobile target localization and tracking," Ph.D. dissertation, Universidad Nacional de Educación a Distancia, Spain, 2013.

[18] S. MartíNez and F. Bullo, "Optimal sensor placement and motion coordination for target tracking," *Automatica*, vol. 42, no. 4, pp. 661–668, 2006.

[19] C. Jauffret, "Observability and fisher information matrix in nonlinear regression," *Aerospace and Electronic Systems, IEEE Transactions on*, vol. 43, no. 2, pp. 756–759, April 2007.

[20] A. P. Aguiar and J. P. Hespanha, "Minimum-energy state estimation for systems with perspective outputs," *Automatic Control, IEEE Transactions on*, vol. 51, no. 2, pp. 226–241, 2006.

[21] A. Shepard, D. Dinsmore, S. Miller, C. Cooper, and R. Wicklund, "Aquarius undersea laboratory: The next generation." 1996.